Sustainable Energy & Fuels

Integration of Electrocatalysts with Silicon Microcone Arrays for Minimization of Optical and Overpotential Losses During Sunlight-Driven Hydrogen Evolution

Journal:	*Sustainable Energy & Fuels*
Manuscript ID	SE-ART-05-2019-000294
Article Type:	Paper
Date Submitted by the Author:	10-May-2019

Complete List of Authors:	Yalamanchili, Sisir; California Institute of Technology, Division of Engineering and Applied Science Kempler, Paul; California Institute of Technology, Division of Chemistry and Chemical Engineering Papadantonakis, Kimberly; California Institute of Technology, Division of Chemistry and Chemical Engineering Atwater, Jr., Harry; California Institute of Technology, Division of Engineering and Applied Science Lewis, Nathan; California Institute of Technology, Division of Chemistry and Chemical Engineering

Integration of Electrocatalysts with Silicon Microcone Arrays for Minimization of Optical and Overpotential Losses During Sunlight-Driven Hydrogen Evolution

Sisir Yalamanchili[1,$], Paul A. Kempler[2,$], Kimberly M. Papadantonakis[2], Harry A. Atwater[1, 3*], Nathan S. Lewis[2-4*]

[1]Division of Engineering and Applied Sciences, California Institute of Technology, Pasadena, CA 91125

[2]Division of Chemistry and Chemical Engineering, California Institute of Technology, Pasadena, CA 91125

[3]Kavli Nanoscience Institute, California Institute of Technology, Pasadena, CA 91125

[4]Beckman Institute, California Institute of Technology, Pasadena, CA 91125

*Corresponding Authors: haa@caltech.edu, nslewis@its.caltech.edu

[$]Equal Contributions

Abstract

Microstructured photoelectrode morphologies can advantageously facilitate integration of optically absorbing electrocatalysts with semiconducting light absorbers, to maintain low overpotentials for fuel production without producing a substantial loss in photocurrent density. We report herein the use of arrays of antireflective, high-aspect-ratio Si microcones (μ-cones), coupled with light-blocking Pt and Co-P catalysts, as photocathodes for H_2 evolution. Thick (~16 nm) layers of Pt or Co-P deposited onto Si μ-cone arrays yielded absolute light-limited photocurrent densities of ~ 32 mA cm^{-2}, representing a reduction in light-limited photocurrent density of 6% relative to bare Si μ-cone-array photocathodes, while maintaining high fill factors and low overpotentials for H_2 production from 0.50 M H_2SO_4(aq). The Si μ-cone arrays were embedded in a flexible polymeric membrane and removed from the Si substrate, to yield flexible photocathodes consisting of polymer-embedded arrays of free-standing μ-cones that evolved hydrogen from 0.50 M H_2SO_4(aq).

Introduction

Microstructured photoelectrodes have several advantages in integrated systems for solar fuel production relative to planar electrodes, including the ability to optimize light absorption and carrier collection in impure, inexpensive semiconductors grown by scalable methods, as well as the ability to support high loadings of electrocatalysts without deleterious absorption of incident photons.[1, 2] Such microstructured materials, utilizing a monolithically integrated tandem absorber configuration, with appropriately integrated electrocatalysts, and embedded in an ionically conductive membrane, can allow for a fully integrated system for water splitting,[3] HI splitting,[4] CO_2 reduction,[5, 6] or N_2 fixation.[7, 8] Electrocatalysts are generally deposited on the light-incident side of the photoelectrode, shadowing the underlying semiconductor and thereby reducing the light-limited current density. When the light absorber and electrocatalyst are both in the optical illumination path, the optimal catalyst loading is therefore determined by the balance between catalyst activity and optical losses due to reflection and parasitic absorption.[9-11]

Bare, planar Si photocathodes exhibit light-limited photocurrent densities $|J_{ph}| < 29$ mA cm^{-2}, due to optical losses arising from front-surface reflection.[12] $|J_{ph}|$ can approach the theoretical maximum of ~ 44 mA cm^{-2} for Si under 100 mW cm^{-2} of Air Mass 1.5 illumination[13] by use of an antireflective coating, combined with surface texturing such as micropyramids (μ–pyramids) produced by anisotropic wet-chemical etching, or by high-aspect-ratio structuring of the Si.[14-17] Antireflective coatings such as SiO_2, Si_3N_4, or Al_2O_3, as commonly used in photovoltaic devices, are not catalytically active or electronically conductive, and are therefore not compatible for use in integrated fuel-producing photoelectrode systems in which charge-transfer occurs across the illuminated solid/liquid interface.[18] Si photocathodes with a passivated front surface and Pt loaded on the rear surface, out of the path of incident light, exhibit

photovoltages in excess of 630 mV under 1 Sun illumination and exhibit limiting photocurrent densities that are relatively independent of the mass loading of electrocatalyst.[19]

Moreover, most of the highly active catalysts for fuel production reflect and parasitically absorb light in the solar spectrum. These optical losses by the catalyst can be reduced by decreasing the catalyst loading to increase transmissivity;[10] by developing transparent and antireflective catalysts;[20, 21] by depositing the catalyst as islands rather than as a continuous film;[22] and/or by strategically placing the catalyst out of the path of incident light on three-dimensionally structured Si substrates.[23] On planar surfaces, increases in the catalyst loading and/or surface coverage decrease the effective current density at the catalyst, so the reduced overpotential and consequent increase in fill factor can partially offset the efficiency losses that would otherwise result from a decrease in $J_{ph.}$[22] The ideal electrode microstructure would therefore simultaneously minimize reflection and absorption losses in the catalyst while optimizing the catalyst loading to reduce the overpotential required to convert photogenerated charge carriers into fuel.

H_2-evolving Si photocathodes have been made using surface texturing such as μ-pyramids, [21, 24] nanowires,[25-28] and microwires (μ-wires).[9-11, 29] Light-limited current densities as high as $|J_{ph}|$ = 43 mA cm^{-2} have been reported for Si μ-pyramids coated with a highly transparent and potentially antireflective MoS_xCl_y catalyst grown by chemical-vapor deposition.[21] A photocurrent density at the reversible hydrogen electrode (RHE) potential, J_{RHE} = -37.5 mA cm^{-2} was obtained for over 30 min, using a transparent $NiCoSe_x$ catalyst formed via light-assisted electrodeposition onto Si nanowire array photocathodes.[28] For Si microwires (μ-wires), J_{RHE} = -35.5 mA cm^{-2} was obtained by optimizing both the coverage of an electrodeposited Ni-Mo catalyst on the μ-wires and the pitch of the μ–wires.[11] Replacing the

catalyst in these structures with thin Pt (~ 5 nm or less), which is widely used because of its high activity and stability in corrosive environments, led to substantial optical absorption and reflection losses, and produced a decrease of 5–7 mA cm^{-2} in $|J_{RHE}|$.[11, 21, 28]

Polymer-embedded Si μ-wires with an antireflective Si_3N_4 coating and scattering particles can absorb up to 84.4% of the incident radiation at normal incidence, which is above the light-trapping limit for an equivalently thick Si substrate.[29, 30] However, widely spaced Si μ-wires on a Si substrate reflect >30% of normally incident light, due to the flat tops of the μ–wires. In contrast, tapering the cylindrical shape of Si μ-wires into Si microcones (μ-cones) with a tip curvature of 25 nm enhances the absorption of Si to > 90% at normal incidence, equivalent to 99.5% of the classical broadband light-trapping limit, with above-the-limit absorption observed at long wavelengths.[16, 17] Such Si μ-cones reflect only ~1% of normally incident light, which is comparable to the reflection from black silicon substrates.[14, 15, 31] This behavior arises from the coupling of broad-band light to multiple available waveguide modes whose resonance exists at various radii resulting from the conical geometry.[17, 32, 33] The high surface area for catalyst loading provided by the μ–cone geometry makes Si μ-cones an attractive architecture for Si photocathodes in hydrogen-producing systems. Herein we investigate the H_2-evolution performance of Si μ-cone array photocathodes coupled with either a highly active but reflective thin film of Pt catalyst, or with a discontinuous film of Co-P as an example of an electrocatalyst comprised of earth-abundant elements. Si μ-cones were removed from the substrate in a flexible polymer support leading to devices which demonstrated H_2 evolution at potentials positive of RHE. Although this work has used Si as proof-of-concept semiconductor, the approach should be extendable to other materials that act as the light-facing high band-gap

component of an integrated tandem photoelectrode structure for photoelectrochemical fuel production (Figure S1).

Results and discussion

Homojunction Si photocathodes with sputtered Pt catalyst

Arrays of Si μ-cones with n^+p homojunctions were prepared by inductively coupled plasma reactive-ion etching (ICP-RIE) of a patterned <100>-oriented p-type Si wafer, followed by diffusion doping with P to form the n^+ emitter layer (experimental details are provided in the Methods section and a schematic of the testing set up is provided in Figure S2). Figure 1 (a-f) schematically shows the fabrication process for the n^+p-Si μ-cone array photocathodes, with the tips of the μ-cones supporting a Pt catalyst (n^+p-Si/Pt μ–cones) for the hydrogen-evolution reaction (HER). Figure 1g shows a scanning-electron micrograph (SEM) of a cross section of an as-prepared n^+p-Si/Pt μ–cone array photocathode with Pt covering 6-9 μm at the tips of the μ-cones.

Figure 2 compares the current density vs potential (*J-E)* behavior under 100 mW cm^{-2} of simulated AM1.5 illumination for varied thicknesses of Pt deposited onto as-fabricated n^+p-Si/Pt μ-cone array photocathodes, planar n^+p-Si/Pt photocathodes, and pyramidally-textured n^+p-Si/Pt photocathodes (μ–pyramid), when operated in contact with H_2-saturated 0.50 M H_2SO_4(aq). Of the three photocathode geometries, the μ–cone array exhibited the highest light-limited photocurrent density $|J_{ph}|$ (at large negative biases, < -1.5 V versus RHE). As expected, the overpotential required for the HER decreased as Pt was added to the photocathodes. For the planar and μ–pyramid geometries, increasing the thickness of the Pt resulted in improvements to the fill factors (*ff*) of the *J-E* characteristic; however, increasing the thickness of the Pt catalyst

beyond 2 nm resulted in reductions to $|J_{ph}|$ due to optical absorption and reflection losses associated with the Pt layer. For the planar and μ–pyramid geometries, $-J_{RHE}$ decreased to < 10 mA cm^{-2} when the thickness of the Pt layer reached 8 nm or 16 nm, respectively. However, Si μ-cone array photocathodes with 8 nm of Pt yielded $-J_{RHE}$ = 33 ± 2 mA cm^{-2}, only ~6% less than $-J_{ph}$ = 35.0 mA cm^{-2} observed for bare n$^+$p-Si μ–cone photocathode arrays (Figure 2d). For n$^+$p-Si/Pt μ–cone array photocathodes with 8 nm of Pt, the voltage required to drive the HER at a rate corresponding to a current density of -10 mA cm^{-2}, V_{-10}, was -70 mV relative to the open-circuit potential (E_{oc}). Doubling the thickness of the Pt layer, from 8 nm to 16 nm, on the tips of the μ–cones resulted in a slight decrease in $-J_{RHE}$, to 31 ± 3 mA cm^{-2}, but did not change V_{-10}. The addition of a titanium adhesion layer between the Si and Pt did not change V_{oc} or V_{-10} and did not produce a decrease in $|J_{ph}|$ relative to the bare n$^+$p-Si μ–cone array. This behavior indicated that either increased reflection into the internal volume of the array, or reduced parasitic absorption due to increased continuity of the film, reduced the optical losses in the catalyst layer. The values of $-V_{-10}$ for planar Si and μ-pyramidal Si photocathodes, 87 mV and 80 mV respectively, were slightly higher than those observed for Si μ-cone arrays with at least 8 nm of Pt, despite complete coverage of the Si surface with 4 nm of Pt. Further increases to the thickness of the Pt, to 8 nm on planar Si, and to 16 nm on μ-pyramidal arrays, led to improved *ff* but resulted in $-J_{ph}$< 10 mA cm^{-2}. Despite the Pt catalyst covering just ~2% of the total surface area of the Si μ–cone array photocathode, the μ-cone geometry maintained a relatively low overpotential while simultaneously exhibiting a value of $-J_{ph}$ that was higher than the values exhibited by bare planar or random μ-pyramidal textured Si photocathodes.

The ideal regenerative cell efficiency (η_{IRC}) represents the efficiency of a photoelectrode operating in conjunction with a nonpolarizable counter electrode performing the reverse reaction

of interest, and was used as a metric to compare the performance of various different photocathodes.[34] The η_{IRC} for n^+p-Si/Pt μ–cone photocathodes with 8 nm of Pt was 5.8 ± 1.1 %, with a best-performing device yielding η_{IRC} = 6.9%. The η_{IRC} for n^+p-Si/Pt μ–cone photocathodes with 16 nm Pt and 4 nm of titanium was 6.7 ± 2.4 %, with a best-performing device yielding η_{IRC} = 9.8% (Figure S3). The use of an n^+p-Si homojunction with 8 nm, 16 nm of Pt, or a Ti/Pt stack on Si μ-cones resulted in an open-circuit potential (E_{oc}) of 416 ± 15 mV, 402 ± 22 mV, and 416 ± 60 mV respectively, vs RHE, and yielded light-limited photocurrent densities at potentials > 0 V vs RHE. The E_{oc} values for the best-performing device were 431 mV for 8 nm Pt films and were 442 mV for 16 nm Pt films. Thus the open-circuit voltage was insensitive to the thickness of the catalyst layer but greater $|J_{ph}|$ was obtained with the inclusion of a Ti adhesion layer separating the Si/Pt interface. The primary difference between the performance of best-performing devices and average devices thus arose from the higher photovoltages of best-performing devices relative to average photocathodes.

The planar and μ-pyramid Si photocathodes showed higher photovoltages than the μ–cone photocathodes (Figure 2), even though all of the photocathodes were diffusion doped by a nominally identical process (see the methods section for details). SEM images indicated that the Si μ–cone arrays had an ~12.5-fold increase in junction area compared to a planar Si electrode, leading to an expected decrease in E_{oc} of ~65 mV assuming a diode quality factor of 1.0.[35, 36] Diffusion-doped, etched Si μ-wire based photocathodes for HER have been reported to exhibit E_{oc} up to 480 mV.[10] The observed E_{oc} of 440 mV for the highest-efficiency photocathodes thus suggests that more voltage was being lost than expected from the increase in surface area. The three-dimensional diffusion of P atoms is likely to preferentially dope the tips of the microcones, which could further enhance the recombination and thus lower the

photovoltage.[37] Hence, optimization of the doping process at the tips of the microcones could potentially improve the photovoltage of similar devices.

When Pt was deposited to a thickness >4 nm, n^+p-Si/Pt photocathodes were stable under air exposure for a few days between fabrication and testing. These electrodes also reversibly passed anodic current, indicating that the Pt layer protected the Si from forming an insulating interfacial oxide layer. After pauses at open circuit, photocathodes with 2-4 nm of Pt exhibited a decrease in η_{IRC} with successive scans, due to a decrease in *ff*. In contrast, n^+p-Si/Pt μ-cone array photocathodes loaded with 16 nm of Pt did not show a decrease in *ff* with successive scans (Figure S4). Even though the catalytic overpotential was not changed by increasing the thickness of Pt beyond 4 nm for n^+p-Si/Pt photocathodes with planar or μ-pyramid geometries, the increased thickness of the Pt layer thus beneficially improved the stability of these electrodes. The increased Pt thickness needed for stability decreased the amount of light transmitted into the Si and limited the photocurrent densities obtainable from n^+p-Si/Pt planar and μ-pyramid photocathodes. In contrast, little or no loss of J_{ph} or *ff* accompanied the increase in Pt thickness (16 nm) required for stable performance of the n^+p-Si/Pt μ-cone array photocathodes. Extended testing of n^+p-Si/Pt μ-cone array photocathodes was performed using chronopotentiometry at -10 mA cm^{-2} (Figure S5). The potential of the photocathode drifted negative with time while E_{oc} remained relatively constant, indicating an increase in V_{-10} at the catalyst. The losses in photocurrent onset could be reversed by cleaning the photoelectrode in concentrated HCl/HNO_3 followed by deionized H_2O (Figure S5). Frequency- and potential-dependent impedance spectroscopy revealed that voltage losses due to ohmic resistance were minimal, and inspection of the catalyst film after evaluation by SEM (Figure S6) did not reveal loss of catalyst from the surface. A detailed discussion is provided in the Supporting Information.

Si photocathodes with electrodeposited Co-P catalyst

Co-P, an earth abundant, active HER electrocatalyst, was used to explore the compatibility of Si μ-cone arrays with catalysts other than noble metals such as Pt. Additionally, on p-type Si, Co-P produces a photovoltage in the absence of a homojunction,[38] providing the opportunity to compare the behavior of systems that have an emitter, in n^+-p structures, with photocathodes that instead primarily rely on minority- carrier collection in the light absorber to determine the spatial location of interfacial photocurrent collection at the solid/catalyst/liquid interface. To fabricate such photocathodes, Co/Co-P was electrodeposited onto Si μ-cones using a narrow-band light-emitting diode with an intensity-averaged wavelength of 625 nm, until a charge density of 400 mC cm^{-2} was passed. The bare p-Si μ-cone arrays predominantly absorbed light at 625 nm at the tips of the μ-cones.[17] Due to deposition at mass-transport-limited current densities, photoelectrodeposition of the Co/Co-P film occurred preferentially at the tips of the Si μ-cones, producing clumps > 1 μm in diameter that shadowed the underlying array (Figure 3a). To obtain an active Co-P catalyst, excess Co was removed by extended potential cycling in contact with 0.50 M H_2SO_4(aq) while under 100 mW cm^{-2} of simulated AM1.5 solar illumination.[38] Potential cycling resulted in a restructuring of the catalyst film into nanoscale islands that were located predominantly at the tips of the μ–cones (Figure 3b).

Figure 4 shows the *J-E* behavior of an illuminated bare p-Si μ–cone array photocathode, as well as the evolution of the *J-E* behavior of a p-Si/Co-P μ–cone array photocathode operated in contact with 0.50 M H_2SO_4(aq). Both J_{ph} and E_{oc} of the p-Si/Co-P μ–cone array photocathode improved with cycling and began to stabilize after ~ 16 voltammetric *J-E* cycles. Deposition of Co-P on planar, μ-pyramid, or μ-wire Si photocathodes yielded $-J_{ph}$ of 15 mA cm^{-2}, 20 mA cm^{-2}, and 25 mA cm^{-2} respectively [38], whereas p-type Si μ-cone/Co-P photocathodes exhibited $-J_{ph}$ =

32 ± 2 mA cm^{-2}. Compared to bare p-type Si μ-cone array photocathodes, the deposition of Co-P on the Si μ-cone tips resulted in an average decrease in $-J_{ph}$ of 3 mA cm^{-2}. Si μ-cone array photocathodes exhibited $-J_{RHE}$ = 29 ± 2 mA cm^{-2} compared to $-J_{RHE}$ = 13 mA cm^{-2}, 18 mA cm^{-2}, and 22 mA cm^{-2} from planar, μ-pyramidal, and μ-wire array Si photocathodes, respectively,[38] demonstrating the beneficial light trapping properties of the Si μ-cone morphology when coupled with the Co-P HER catalyst.

The average E_{oc} for the p-Si/Co-P μ-cone array photocathodes was 331 ± 50 mV vs RHE, and the highest observed E_{oc} for the p-Si/Co-P μ-cone photocathodes was 384 mV vs RHE. The p-Si/Co-P μ-cone array photocathodes did not require a diffusion-doped homojunction but yielded lower E_{oc} values than the n^+p-Si/Pt μ-cone array photoelectrodes. The p-Si/Co-P μ-cone array photocathodes reached a solar-to-fuel current density of -10 mA cm^{-2} at +197 ± 20 mV vs RHE. A best-performing device exhibited this current density at +220 mV versus RHE, with η_{IRC} = 3.1% (Figure S7). This efficiency is comparable to the value obtained from the Si μ-wire morphology and is higher than the values reported for planar and μ-pyramid Si photocathodes (Table 1).[38] Extended testing of p-Si/Co-P μ-cone array photocathodes at 0 V vs RHE showed that after the initial increase in $|J_{ph}|$ during the first 30 min of cycling, the optical properties of the device remained stable for 24 h (Figure S8). SEM images of electrodes before and after extended testing in 0.50 M H_2SO_4(aq) showed that the structure of the Si μ-cone array was unchanged whereas the Co-P catalyst layer had restructured from μm-scale particles to nanoscale islands (Figure S9).

Figure 5a compares the reflectance in the wavelength range of 400 nm – 1100 nm for bare Si μ-cone array, a Si μ-cone array with 8 nm or 16 nm of Pt selectively deposited at the tips of the μ-cones, and a p-Si/Co-P μ-cone array electrode. No substantial change was observed in

reflectance between n^+p-Si μ-cone arrays with and without a Pt coating, indicating that the incident light that is typically reflected from planar or μ-pyramid Si surfaces was redirected into the Si substrate due to the conical geometry. Figure S10 compares the reflectance of the μ-cone arrays to the μ-pyramids, showing that the conical geometry had ~15-20% lower reflectance in 400-1100 nm range. Hence, the Si μ-cone arrays had superior light-trapping properties relative to the bare Si pyramid structures before and after deposition of the catalyst. This concept is similar to that observed previously in effectively transparent contacts for silicon solar cells.[39-41] The reflectance of the p-Si/Co-P μ-cone array was 5% higher than the reflectance of the n^+p-Si/Pt μ-cone array because the Co-P islands were rough compared to the sputtered Pt coating, allowing relatively higher outward scattering of light from the Co-P islands on the tips of the μ-cones. Although the p-Si/Co-P μ-cones exhibited higher reflectance than the Pt-loaded μ-cones, the average J_{ph} was the same (-32 mA cm^{-2}) for p-Si/Co-P μ-cone arrays and n^+p-Si/Pt μ-cone arrays with 16 nm of Pt, indicating that in the 400 nm – 1100 nm wavelength range, 16 nm of Pt has a higher parasitic absorption than Co-P. Figure 5b compares the spectral response of an n^+p-Si/Ti/Pt μ-cone array to a p-Si/Co-P μ-cone array in 0.50 M H_2SO_4(aq) at 0 V and -0.2 V vs RHE, respectively. Both photocathodes exhibited external quantum yields, defined as the fraction of photons collected as photocurrent, $\phi_{ext}(\lambda)$, in excess of 0.8 for wavelengths between 450-900 nm. The integrated photocurrent density for the AM1.5 spectrum was calculated via Equation 1:

$$J_{ph} = \frac{q}{hc}\int_{400\text{ nm}}^{1100\text{ nm}} \phi_{ext}(\lambda) \cdot P_{AM1.5}(\lambda) \cdot d\lambda \qquad (1)$$

where $P_{AM1.5}(\lambda)$ is the power density per cm^2 of the AM1.5 spectrum at the specified wavelength. The predicted limiting photocurrent density under AM1.5 illumination was in excellent accord with the measured J_{ph}.

Bare p-type Si μ-cone arrays were also embedded in polydimethylsiloxane (PDMS), peeled off the substrate, and fabricated into electrodes by deposition of a Au back contact using electron-beam evaporation (see Methods for more detail). Figure 3c shows a SEM image of Si μ-cone arrays in PDMS with ~ 15 μm of the tips exposed, with the freestanding, polymer-embedded μ-cones arrays decorated with Co-P using the same procedure as described for the on-substrate p-type Si μ-cones. Free-standing devices were tested as photocathodes in 0.50 M H_2SO_4(aq), to evaluate the performance of μ-cones in a membrane-embedded photocathode for H_2(g) generation. Figure 6 presents representative *J-E* data in 0.50 M H_2SO_4(aq) under 100 mW cm^{-2} of simulated AM1.5 illumination. These devices exhibited E_{oc} = 150 ± 36 mV and J_{RHE} = -0.94 ± 0.32 mA cm^{-2}, with a best-performing device exhibiting J_{RHE} = -1.41 mA cm^{-2}. At -200 mV vs RHE, free-standing Si μ-cones exhibited an average J_{ph} = -6.5 mA cm^{-2}, and the best-performing device exhibited J_{ph} = -8.1 mA cm^{-2} and remained active for 3 h of testing. The photoactivity indicated that many of the individual p-type Si μ-cones were directly contacted with electrolyte during the Co-P catalyst deposition, and also while being tested as photocathodes. The absolute photocurrent density was higher than previous reports for Si μ-wires embedded in polymer membranes,[4, 9, 42] but lower than the photocurrent density for Si μ-cones on a substrate. Incomplete contact between the Au back contact and individual Si μ-cones may be responsible for the reduced photon collection of the free-standing array fabricated for proof-of-concept purposes in this work. Further optimization of the placement of the catalysts,

to more optimally match local carrier generation rate, could be achieved using light-guided deposition of catalysts.[43]

The p-Si μ-cone/Co-P photocathodes do not require formation of a homojunction or emitter layer, thereby reducing the need for high temperature processing. Use of surface passivation and/or a homojunction or amorphous silicon heterojunction on the Si μ-cone arrays could thus improve the efficiency by reducing surface recombination velocities while retaining the benefit of high light absorption in Si μ-cones. Si μ-cones with < 100 cm s^{-1} surface passivation can in principle produce E_{oc} > 650 mV,[16, 17] and membrane-embedded μ-cones absorb > 90% of the light relative to their on-substrate counterpart. Polymer-embedded Si μ-cone arrays could thus produce $-J_{ph}$ > 25 mA cm^{-2}. Under standard conditions, HI splitting requires a minimum voltage of ~ 0.53 V, so utilizing a highly active catalyst such as Pt for the HER, along with improving the current collection could lead to flexible membrane-embedded photocathodes for HI splitting potentially reaching η_{IRC} > 10%.

Microcone array photoelectrodes can in principle be fabricated in a scalable manner over large areas either by controlled electrochemical etching and/or by transferring the microcone arrays into peeled polymer films with subsequent re-use of the patterned growth substrate.[44] The approach of structuring a photoelectrode, in which both the absorber and electrocatalyst are in the illumination path, into microcone arrays provides a general strategy for optimization of light absorption in the photoelectrode without producing obscuration by high mass loadings of optically absorbing and/or reflecting electrocatalyst films often required for the low-overpotential production of fuel and/or for efficient water oxidation to O_2(g). Photoelectrodes utilizing Si μ-cones could additionally be implemented as a tandem junction to produce photovoltages necessary for water-splitting, with a wider band gap material deposited on the

surface of the cones, in a similar fashion to previous studies that used a core-shell design on Si microwire arrays (Figure S1).[45, 46] In a core-shell tandem device, both semiconductors and one of two electrocatalysts would be on the sunlight-facing side of the membrane. Mesoscale metal films avoid parasitic absorption of photons due to resonant coupling,[41] thus Si μ-cone arrays are an advantageous scaffold for integrating wide band gap semiconductors in an architecture which can minimize reflection by the electrocatalyst in the illumination path.

Designs that utilize planar photoelectrodes integrated in a monolithic stack have consistently demonstrated the highest efficiencies for unassisted water splitting.[3, 47, 48] In microstructured electrodes, losses due to the increased area available for recombination at the charge-separating junction lead to lower photovoltages in comparison to planar devices.[19] GaAs microcells that have been transfer printed following epitaxial growth onto devices that used separate surfaces for light absorption and catalysis exhibited high efficiencies when normalized to the active area of the photovoltaics.[49] Printed assemblies of high-efficiency photovoltaics, wired to catalysts that are outside the optical path of incident light, thus could be integrated with ion-exchange membranes to ensure long term, stable sunlight-driven water splitting. However, such devices will necessarily encounter losses in active area when integrating the electrocatalysts and ion conducting membranes necessary for efficient and safe operation, limiting the maximum achievable photocurrent density from such systems. The increased theoretical photocurrent density that could be obtained by appropriately integrated mesoscale-structured semiconductors, electrocatalysts, and ion-exchange membranes may be able offset the losses in photovoltage associated with structured semiconductors, motivating further study into such systems.

Conclusions

High photocurrent densities were exhibited by n^+p-Si/Pt and p-Si/Co-P μ-cone array photocathodes when either Pt or Co-P hydrogen-evolution catalysts were deposited on the tips of the μ–cones. N^+p-Si/Pt μ–cone array photocathodes yielded an average η_{IRC} of 5.7% at the maximum power point, and best-performing n^+p-Si/Ti/Pt μ–cone devices yielded η_{IRC} = 9.8%. Thick (~16 nm) Pt and Co-P deposited onto Si μ-cone arrays produced only a 6% reduction in photocurrent density compared to bare photocathodes having the same morphology and microstructure. However, the Si μ–cone arrays exhibited photovoltages that were lower by > 100 mV than the photovoltages obtained on planar or μ-pyramidally textured Si photocathodes. The photovoltage of the Si μ-cone arrays may be improved by optimizing the homojunction doping distribution. Greater than 90% of the incident light is absorbed in the μ–cones, as opposed to by the p-Si substrate at the base of the μ–cones,[16, 17] so removal of the μ–cones from the substrate will result in confinement of light in an effectively thin silicon absorber layer, facilitating that higher photovoltages from the μ–cone arrays provided that surface recombination can be minimized.[39] The p-Si/Co-P devices showed an average open-circuit voltage of 331 mV vs RHE without an emitter, which in combination with J_{ph} = -32 mA cm^{-2} resulted in η_{IRC} = 3.1%. Substantial improvements to the photovoltage obtained at the Si/Co-P junction will be required for such μ–cone arrays to be used as a practical photocathode in a tandem device. As a proof of concept, Si μ-cone arrays were also embedded in a flexible polymeric membrane, allowing for high catalyst loadings with minimal losses in photocurrent due to catalyst obscuration, and operation in a form factor which could facilitate integration into a tandem device for unassisted sunlight-driven water splitting.

Methods

Fabrication of n^+p-Si μ–cone photocathodes with Pt: Czochralski-grown p-type Si wafers with a <100> orientation and a resistivity of 0.60-0.80 ohm-cm (Addison Engineering, Inc.) were photolithographically patterned with a square grid of Al_2O_3 circles that were 3 μm in diameter with a 7 μm pitch. The Al_2O_3 was deposited to a thickness of 200 nm via electron-beam evaporation. The μ–cones were etched from the masked p-Si wafer using an Oxford Dielectric System 100 ICP/RIE following a procedure described previously.[39] A capacitively coupled power of 7 W, and an inductively coupled power of 900 W, was used for etching. Etching was performed in three steps, in which the ratio of SF_6 to O_2 gas was varied stepwise from 70 sccm : 6 sccm to 70 sccm : 7 sccm by increasing the rate of O_2 flow by 0.5 sccm every 30 min. The chamber temperature and pressure were maintained at -130 ^oC and 10 mTorr, respectively. After etching, samples were cleaned via a modified RCA standard clean 1 (5:1:1 (vol) H_2O:NH_4OH:H_2O_2 at 70 °C) followed by an RCA standard clean 2 (6:1:1 (vol) H_2O:HCl:H_2O_2 at 70 °C). The samples were dipped in HF between the cleaning steps, which also resulted in removal of the Al_2O_3 etch mask. After cleaning, the samples were dipped in ~ 6.5 M HF(aq) for 1 min before thermal P diffusion using a Saint-Gobain PH-900 PDS diffusion-doping source at 850 ^oC for 15 min under a N_2(g) ambient, to yield an n^+p homojunction. To reduce thermal stresses, the samples were inserted into, and removed from, the doping furnace over the course of 1 min. The Si μ–cones were then heated to 150 ^oC on a hot plate, and mounting wax (Quickstick 135, South Bay Tech) was melted into the array as a mask. Excess wax was removed by reactive-ion etching using an O_2 plasma at a forward power of 400 W and 300 mTorr operating pressure. The wax was etched until 6-9 μm of the tips of the μ-cones were exposed. The samples were then dipped in ~ 6.5 M HF for ~1 min to remove the native oxide over the Si μ–cones, and Ti and/or Pt were sputtered onto the samples. The reproducible sputtering rate of

the system allowed for the thickness to be controlled by the sputtering time and was referenced to a planar control wafer. Metal thicknesses on planar samples were measured with a DektakXT Profilometer. The samples were then immersed in acetone and sonicated for 15 min to completely remove the wax, resulting in Si μ–cones with metal selectively deposited over the tips of the μ–cones. To make bottom-facing electrodes, In-Ga (Alfa Aesar) was scratched into the back sides of Si μ–cone chips, and a Cu-Sn wire was affixed to the In-Ga using as an adhesive Ag paint having a grain size < 1.0 μm (PELCO, Ted Pella). The Cu-Sn wire was fed through 6 mm outer diameter borosilicate glass tubing that was 1 mm thick, and the electrically contacted chips were sealed onto the end of the tubing using an opaque, insulating epoxy (Hysol 9460) that was allowed to cure at room temperature for > 12 h or at 80 °C for 6 h.

Fabrication of p-Si μ-cone photocathodes with Co-P: p-Si μ–cone arrays were fabricated via the above etching and cleaning procedures but were not doped with an n^+ emitter layer. Bottom-facing electrodes were made from the p-Si μ–cones as described in the previous section, and Co/Co-P was photoelectrochemically deposited onto the surface of the p-Si μ–cones using illumination from a narrowband light-emitting diode (LED) (Thorlabs) with an intensity-averaged wavelength of 625 nm. The light intensity at the surface of the sample was ~200 mW cm^{-2}. The Co/Co-P plating bath has been described elsewhere,[50] and was purged vigorously with Ar(g) prior to and during the deposition, with a gas stream in close proximity to the sample to drive local convection.

Fabrication of membrane-embedded p-Si μ-cone photocathodes with Co-P: p-Si μ-cones were embedded in PDMS by spin coating a 10:10:1 (vol) solution of toluene, PDMS elastomer, and curing agent (Dow Sylgard™ 184) at 3000 rpm, leaving the top ~15 μm of the μ-cones exposed. The samples were cured on a hot plate at 150 °C for ~ 30 min. The μ-cones were

peeled off of the substrate using a razor blade. The flexible polymer membrane was held on its edges sandwiched between Kapton tape and a glass slide, with the back side of the μ-cones facing up. The thickness of the tape ensured that the tips of the μ-cones were not damaged. 500 nm of Au was deposited via electron-beam evaporation onto the backs of the μ-cones. Electrodes were made using these flexible substrates with Ag ink connecting the Au back contact to a Cu-Sn wire that was fed through 6 mm outer diameter borosilicate glass tubing which was 1 mm thick. The electrodes were then sealed using an opaque, insulating epoxy (Hysol 9460) that was allowed to cure at room temperature for > 12 h or at 80 °C for 6 h. Co-P was electrodeposited under similar conditions to those used for the on-substrate samples.

(Photo)electrochemical measurements: The performance of photocathodes for photoelectrochemical hydrogen evolution was measured in H_2-purged 0.50 M H_2SO_4(aq) (TraceMetals grade, Fisher) under 100 mW cm^{-2} of simulated AM1.5 illumination produced by a filtered Hg (Xe) lamp powered at 290 W (Figure S2). A Biologic SP-200 was used for the potentiostat, and the electrochemical cell had a three-electrode configuration. A Ag/AgCl (Saturated KCl) or Saturated Calomel reference electrode was calibrated against the RHE potential using a platinum-black electrode, and a graphite rod positioned behind a porous glass frit served as the counter electrode. Current density vs potential, *J-E*, data were obtained by sweeping the potential at 50 mV s^{-1} from open circuit to -0.2 V vs RHE. The electrolyte was stirred rapidly with a magnetic stir bar, to remove hydrogen bubbles from the surface of the device.

Spectral response measurements: The external quantum yield of n^+p-Si/Ti/Pt and p-Si/Co-P μ–cone arrays were recorded using a Biologic VMP3 Multichannel potentiostat connected to a lock-in amplifier with illumination from a Xe lamp powered at 150 W passed through a

monochromator controlled via LabView and chopped at 10-15 Hz. Spectra were referenced to a calibrated reference diode (Thorlabs FDS100-CAL). The potential of p-Si/Co-P photocathodes was held at -200 mV vs RHE to ensure that the sample remained under reductive bias in the dark, while the potential of n^+p-Si/Ti/Pt photocathodes was held at 0 V vs RHE.

Author Information

Author Contributions
[$]These authors contributed equally (SY and PAK)

Corresponding Authors

*Email: haa@caltech.edu
nslewis@caltech.edu

Conflicts of Interest

The authors declare no competing financial interest.

Acknowledgments

This material is based upon work performed by the Joint Center for Artificial Photosynthesis, a DOE Energy Innovation Hub, as follows: electrochemical measurements for all devices, and fabrication of p-Si/Co-P devices was supported through the Office of Science of the U.S. Department of Energy under Award No. DE- SC0004993; the development and fabrication of p-Si and n^+p-Si/Pt μ-cone arrays and reflection measurements were supported by the National Science Foundation (NSF) under NSF CA No. EEC-1041895. Additional support for this work was provided by the Lockheed Martin Corporation (Award 4103810021). Fabrication of Si μ-cones was performed in the Kavli Nanoscience Institute (KNI) at Caltech, and we thank the KNI staff for their assistance during fabrication.

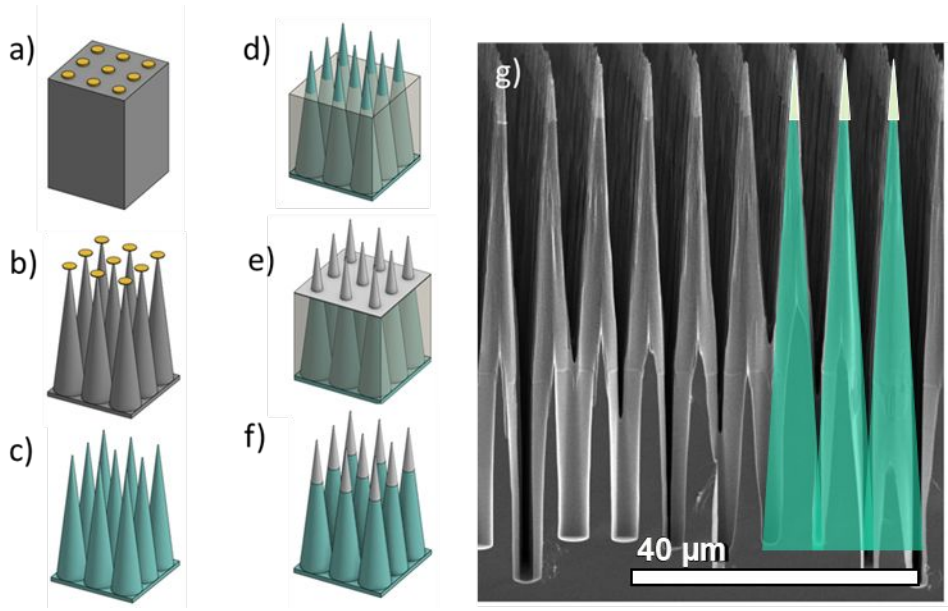

Figure 1: Schematic for the fabrication of n^+p-Si µ–cone array photocathodes with Pt selectively loaded on the tips of the µ-cones. (a) Aluminum oxide mask (yellow) patterned on p-type silicon (gray). (b) Controlled undercutting of the etch mask leads to high-aspect-ratio cones. (c) Removal of the etch mask followed by formation of an n^+-emitter layer (green) via phosphorus doping. (d) Infilling with wax (transparent gray) followed by directional O_2 etching to expose tips. (e) Uniform deposition of Pt via sputtering. (f) Removal of the wax with acetone leaves Pt only at the cone tips. (g) Scanning-electron micrograph of n^+p-Si µ–cone photocathodes with Pt selectively deposited on the tips of the µ-cones.

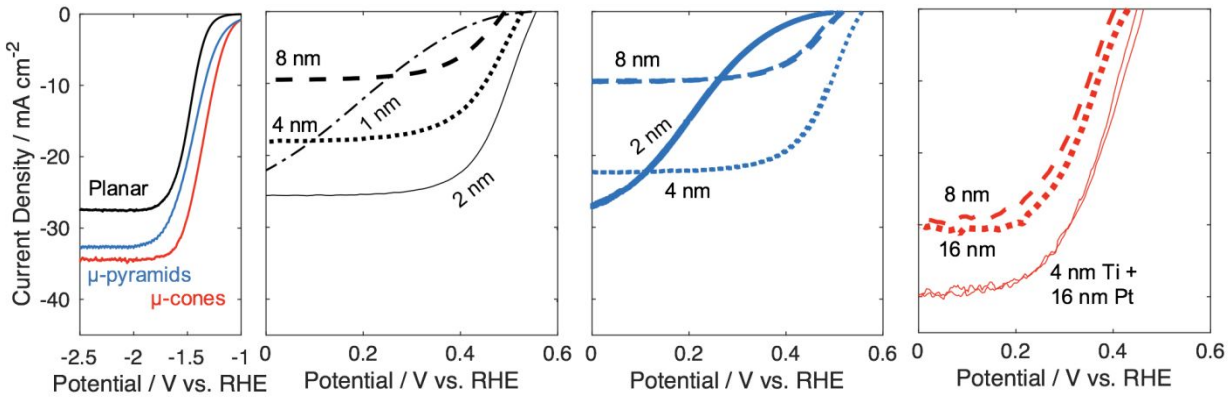

Figure 2: Effect of Pt loading on the *J-E* behavior of n^+p-Si photocathodes with planar (black traces), μ-pyramid (blue traces), and μ-cone array (red traces) morphologies, as measured in contact with H_2-saturated 0.50 M H_2SO_4(aq) while illuminated by 100 mW cm^{-2} of simulated Air Mass (AM) 1.5 illumination. (a) *J-E* behavior of bare (no Pt) n^+p-Si photocathodes. Representative *J-E* behavior for n^+p-Si/Pt photocathodes with varied Pt loadings for the (b) planar, (c) μ–pyramid and (d) μ–cone morphologies.

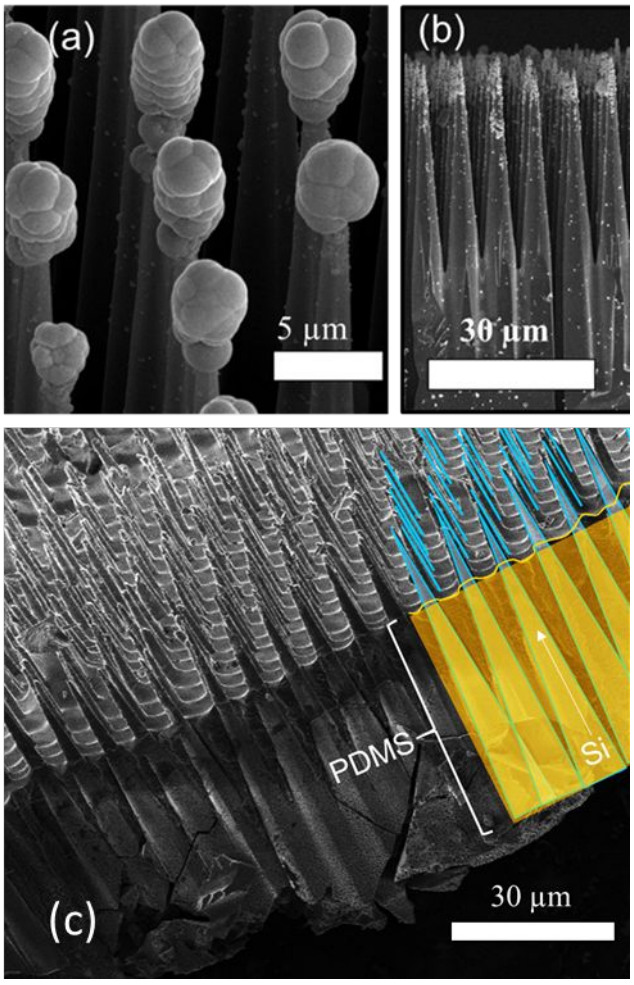

Figure 3: (a) Scanning-electron micrograph (SEM) of as-deposited Co/Co-P photoelectrodeposited onto the tips of p-Si μ-cones. The Co/Co-P loading, as determined by the charge density passed during the photoelectrodeposition, was 400 mC cm^{-2}. (b) SEM image of a cross section of a p-Si/Co-P μ–cone array after removal of excess Co by potential cycling in 0.50 M H_2SO_4(aq). (c) SEM of polymer embedded Si μ-cones removed from substrate, after deposition of Co-P and potential cycling in 0.50 M H_2SO_4(aq).

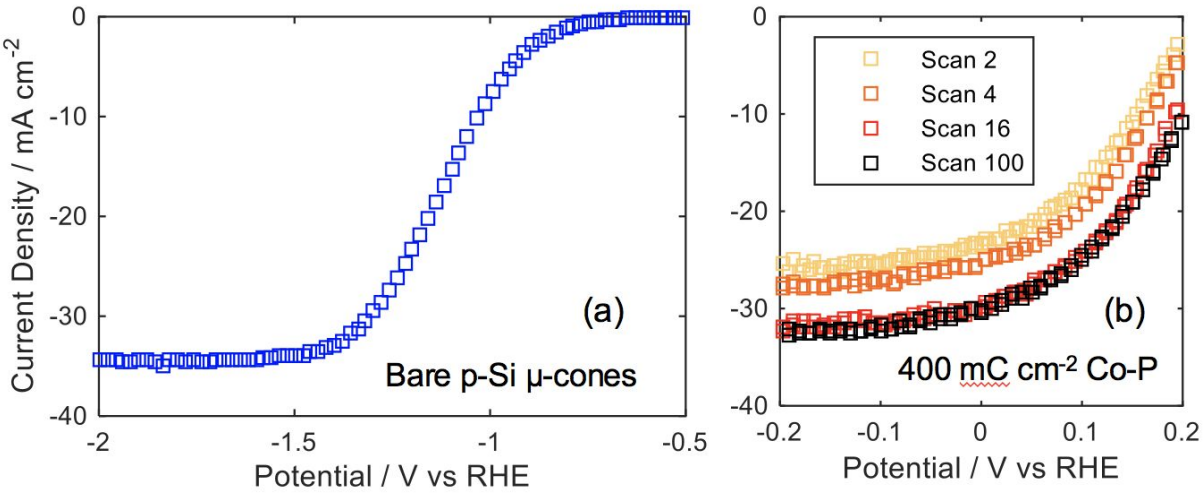

Figure 4: Evolution of the *J-E* behavior of a photocathode consisting of a p-Si/Co-P μ-cone array, when immersed in H_2-saturated 0.50 M H_2SO_4(aq) and illuminated with 100 mW cm^{-2} of simulated AM1.5 illumination with rapid stirring, compared to the same p-Si μ-cone array photocathode prior to catalyst deposition (panel a). b) Effects of extended potential cycling in contact with 0.50 M H_2SO_4(aq) under 1-sun illumination on the *J-E* behavior of a p-Si μ–cone array photocathode loaded with Co/CoP after 2, 4, 16, and 100 scans from -0.376 V to +0.224 V vs RHE at 50 mV s^{-1}. The first and last scans were recorded after 20 s and 40 min, respectively.

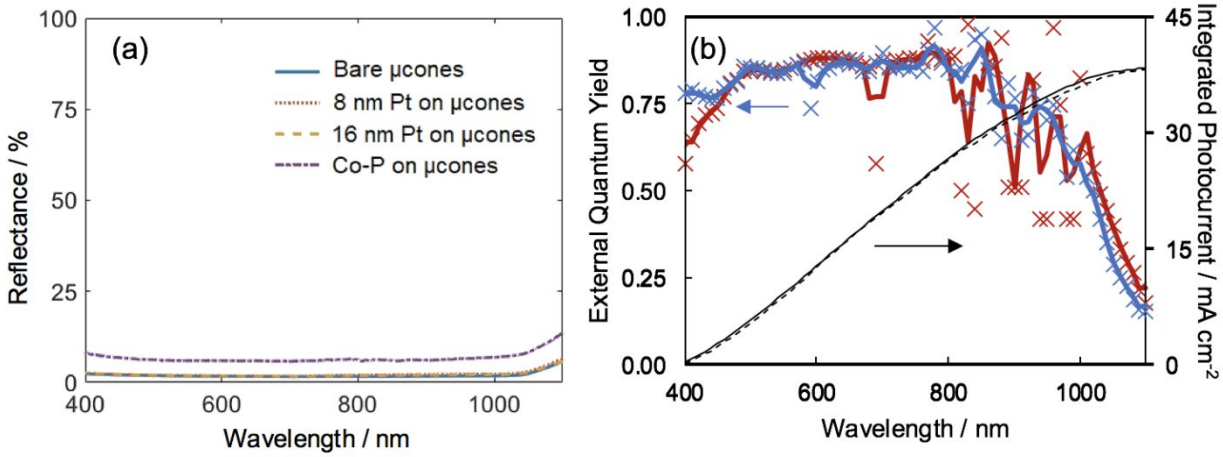

Figure 5: (a) Reflectance measurement of bare Si μ-cone arrays, Si μ-cone arrays with 8 and 16 nm of Pt or Co-P on their tips, as measured using a Cary 5000 UV-Vis-NIR with an integrating sphere. (b) Spectral response of a n^+p-Si/Pt μ-cone array at 0 V RHE (red) and p-Si μ-cone array in with 400 mC cm^{-2} Co-P at -200 mV vs RHE after activation in H_2 saturated 0.50 M H_2SO_4 for 30 min (blue). Individual data points were recorded every 10 nm, with a continuous line plotting the midpoint average for three data points. The maximum integrated photocurrent is plotted as a black line for a p-Si/Co-P μ-cone array (continuous) and n^+p-Si/Pt μ-cone array (dashed) from 400 nm to 1100 nm based on the photon density of the AM1.5 spectrum.

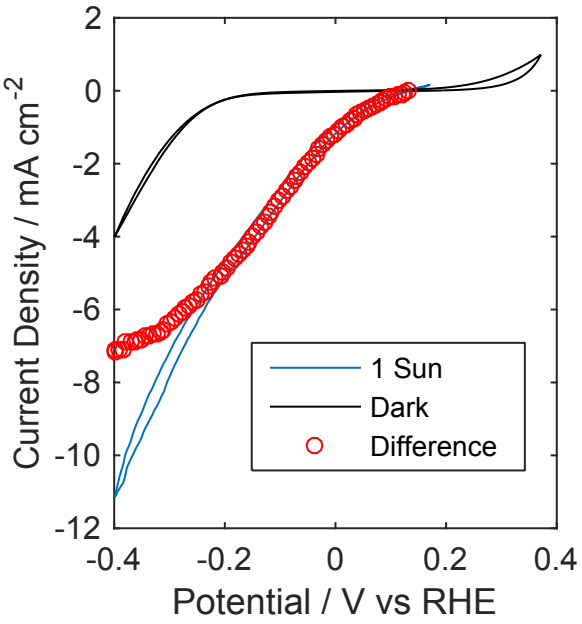

Figure 6: Representative *J-E* behavior of PDMS-embedded Si μ–cone array photocathodes decorated with Co-P and tested in 0.50 M H_2SO_4(aq) under 100 mW cm^{-2} of simulated AM1.5 illumination (blue). For comparison, the *J-E* behavior was recorded in the absence of illumination (black), and the difference between the two measured values was taken to be the photocurrent density for a given potential (red circle)

Tables

Device Type	J_{RHE} *(mA cm^{-2})*	J_{ph} *(mA cm^{-2})*	E_{oc} *(mV)*	η_{IRC} *(%)*	η_{IRC}* *(%)*
n^+p-Si μ–cones, 8 nm Pt	-33 ± 2	-34 ± 2	416 ± 14	5.8 ± 1.0	6.9
n^+p-Si μ–cones, 16 nm Pt	-31 ± 3	-32 ± 3	402 ± 20	5.6 ± 1.0	7.4
n^+p-Si μ–cones, 4 nm Ti/16 nm Pt	-35 ± 3	-36 ± 3	416 ± 60	6.7 ± 2.4	9.8
n^+p-Si Planar 4nm Pt	-17 ± 1	-17 ± 1	539 ± 9	5.4 ± 0.4	5.7
n^+p-Si μ-pyramids, 4 nm Pt	-24 ± 3	-24 ± 3	533 ± 15	6.9 ± 1.3	8.0
n^+p-Si μ-pyramids, 16 nm Pt	-9.1 ± 1.3	-9.1 ± 1.3	519 ± 9	2.8 ± 0.3	3.0
p-Si μ–cones, Co-P	-29 ± 2	-32 ± 2	331 ± 44	2.7 ± 0.3	3.1
*p-Si μ-pyramids, Co-P***	-18 ± 1	-20	286 ± 11	-	-
*p-Si planar, Co-P***	-13 ± 1	-15	265 ± 26	0.82 ± 1.3	0.98
*p-Si μ-wires, Co-P***	-22 ± 2	-25	342 ± 24	2.4 ± 0.1	2.5
p-Si μ-cones, Bare	-	-35	-	-	-
p-Si μ-pyramid, Bare	-	-31	-	-	-
p-Si planar, Bare	-	-28	-	-	-

Table 1: Summary of performance metrics for planar, μ-pyramid, and μ-cone array photocathodes measured in contact with H_2-saturated 0.50 M H_2SO_4(aq). Average values and standard deviations (in parentheses) were calculated from measurements of at least 3 separate photoelectrodes. The light-limited current density, J_{ph}, was measured at -200 mV vs RHE; the current density at the formal potential of the H^+/H_2 redox system, J_{RHE}, was measured at 0 V vs RHE. E_{oc} is reported relative to RHE. * indicates performance of best-performing devices, and ** indicates values from a previous study.[38]

References

1. B. M. Kayes, H. A. Atwater and N. S. Lewis, *J. Appl. Phys.*, 2005, **97**, 114302.
2. E. L. Warren, H. A. Atwater and N. S. Lewis, *J. Phys. Chem. C*, 2014, **118**, 747-759.
3. E. Verlage, S. Hu, R. Liu, R. J. Jones, K. Sun, C. Xiang, N. S. Lewis and H. A. Atwater, *Energy Environ. Sci.*, 2015, **8**, 3166-3172.
4. S. Ardo, S. H. Park, E. L. Warren and N. S. Lewis, *Energy Environ. Sci.*, 2015, **8**, 1484-1492.
5. B. Kumar, M. Llorente, J. Froehlich, T. Dang, A. Sathrum and C. P. Kubiak, *Annu. Rev. Phys. Chem.*, 2012, **63**, 541-569.
6. J. L. White, M. F. Baruch, J. E. Pander, Y. Hu, I. C. Fortmeyer, J. E. Park, T. Zhang, K. Liao, J. Gu, Y. Yan, T. W. Shaw, E. Abelev and A. B. Bocarsly, *Chem. Rev.*, 2015, **115**, 12888-12935.
7. M. Ali, F. Zhou, K. Chen, C. Kotzur, C. Xiao, L. Bourgeois, X. Zhang and D. R. MacFarlane, *Nat. Comm.*, 2016, **7**, 11335.
8. T. Oshikiri, K. Ueno and H. Misawa, *Angew. Chem. Int. Ed.*, 2014, **53**, 9802-9805.
9. E. L. Warren, J. R. McKone, H. A. Atwater, H. B. Gray and N. S. Lewis, *Energy Environ. Sci.*, 2012, **5**, 9653-9661.
10. C. W. Roske, E. J. Popczun, B. Seger, C. G. Read, T. Pedersen, O. Hansen, P. C. K. Vesborg, B. S. Brunschwig, R. E. Schaak, I. Chorkendorff, H. B. Gray and N. S. Lewis, *J. Phys. Chem. Lett.*, 2015, **6**, 1679-1683.
11. W. Vijselaar, P. Westerik, J. Veerbeek, R. M. Tiggelaar, E. Berenschot, N. R. Tas, H. Gardeniers and J. Huskens, *Nat. Energy*, 2018, **3**, 185-192.
12. K. R. McIntosh and S. C. Baker-Finch, 2012 38th IEEE Photovoltaic Specialists Conference, 2012.
13. S. Rühle, *Solar Energy*, 2016, **130**, 139-147.
14. S. J. Cho, T. An and G. Lim, *Chem. Commun.*, 2014, **50**, 15710-15713.
15. X. Liu, P. R. Coxon, M. Peters, B. Hoex, J. M. Cole and D. J. Fray, *Energy Environ. Sci.*, 2014, **7**, 3223-3263.
16. S. Yalamanchili, H. S. Emmer, N. S. Lewis and H. A. Atwater, 2016 IEEE 43rd Photovoltaic Specialists Conference (PVSC), 2016.
17. S. Yalamanchili, H. S. Emmer, K. T. Fountaine, C. T. Chen, N. S. Lewis and H. A. Atwater, *ACS Photonics*, 2016, **3**, 1854-1861.
18. A. Vázquez-Guardado, J. Boroumand, D. Franklin and D. Chanda, *Phys. Rev. Mat.*, 2018, **2**, 035201.

19. H.-P. Wang, K. Sun, S. Y. Noh, A. Kargar, M.-L. Tsai, M.-Y. Huang, D. Wang and J.-H. He, *Nano Lett.*, 2015, **15**, 2817-2824.
20. Z. Chen, S. Ye, A. R. Wilson, Y.-C. Ha and B. J. Wiley, *Energy Environ. Sci.*, 2014, **7**, 1461-1467.
21. Q. Ding, J. Zhai, M. Cabán-Acevedo, M. J. Shearer, L. Li, H. C. Chang, M. L. Tsai, D. Ma, X. Zhang and R. J. Hamers, *Adv. Mater.*, 2015, **27**, 6511-6518.
22. Y. Chen, K. Sun, H. Audesirk, C. Xiang and N. S. Lewis, *Energy Environ. Sci.*, 2015, **8**, 1736-1747.
23. M. R. Shaner, J. R. McKone, H. B. Gray and N. S. Lewis, *Energy Environ. Sci.*, 2015, **8**, 2977-2984.
24. M. Cabán-Acevedo, M. L. Stone, J. R. Schmidt, J. G. Thomas, Q. Ding, H.-C. Chang, M.-L. Tsai, J.-H. He and S. Jin, *Nat. Mat.*, 2015, **14**, 1245.
25. X.-Q. Bao, M. Fatima Cerqueira, P. Alpuim and L. Liu, *Chem. Commun.*, 2015, **51**, 10742-10745.
26. P. Dai, J. Xie, M. T. Mayer, X. Yang, J. Zhan and D. Wang, *Angew. Chem. Int. Ed.*, 2013, **52**, 11119-11123.
27. I. Oh, J. Kye and S. Hwang, *Nano Lett.*, 2012, **12**, 298-302.
28. H. Zhang, Q. Ding, D. He, H. Liu, W. Liu, Z. Li, B. Yang, X. Zhang, L. Lei and S. Jin, *Energy Environ. Sci.*, 2016, **9**, 3113-3119.
29. M. D. Kelzenberg, S. W. Boettcher, J. A. Petykiewicz, D. B. Turner-Evans, M. C. Putnam, E. L. Warren, J. M. Spurgeon, R. M. Briggs, N. S. Lewis and H. A. Atwater, *Nat. Mat.*, 2010, **9**, 239.
30. E. Yablonovitch, *J. Opt. Soc. Am.*, 1982, **72**, 899-907.
31. L. Sainiemi, V. Jokinen, A. Shah, M. Shpak, S. Aura, P. Suvanto and S. Franssila, *Adv. Mater.*, 2011, **23**, 122-126.
32. K. T. Fountaine, C. G. Kendall and H. A. Atwater, *Opt. Express*, 2014, **22**, A930-A940.
33. K. T. Fountaine, W.-H. Cheng, C. R. Bukowsky and H. A. Atwater, *ACS Photonics*, 2016, **3**, 1826-1832.
34. R. H. Coridan, A. C. Nielander, S. A. Francis, M. T. McDowell, V. Dix, S. M. Chatman and N. S. Lewis, *Energy Environ. Sci.*, 2015, **8**, 2886-2901.
35. P. Mialhe, J. P. Charles, A. Khoury and G. Bordure, *J. Phys. D: Appl. Phys.*, 1986, **19**, 483.
36. S. Yalamanchili, N. S. Lewis and H. A. Atwater, 2018 IEEE 7th World Conference on Photovoltaic Energy Conversion (WCPEC) (A Joint Conference of 45th IEEE PVSC, 28th PVSEC & 34th EU PVSEC), 2018.

37. B. Min, H. Wagner, A. Dastgheib-Shirazi, A. Kimmerle, H. Kurz and P. P. Altermatt, *Phys. Status Solidi RRL*, 2014, **8**, 680-684.
38. P. A. Kempler, M. A. Gonzalez, K. M. Papadantonakis and N. S. Lewis, *ACS Energy Lett.*, 2018, **3**, 612-617.
39. R. Saive, C. R. Bukowsky, S. Yalamanchili, M. Boccard, T. Saenz, A. M. Borsuk, Z. Holman and H. A. Atwater, 2016 IEEE 43rd Photovoltaic Specialists Conference (PVSC), 2016.
40. R. Saive, A. M. Borsuk, H. S. Emmer, C. R. Bukowsky, J. V. Lloyd, S. Yalamanchili and H. A. Atwater, *Adv. Opt. Mat.*, 2016, **4**, 1470-1474.
41. R. Saive, M. Boccard, T. Saenz, S. Yalamanchili, C. R. Bukowsky, P. Jahelka, Z. J. Yu, J. Shi, Z. Holman and H. A. Atwater, *Sustainable Energy Fuels*, 2017, **1**, 593-598.
42. D. B. Turner-Evans, H. Emmer, C. T. Chen and H. A. Atwater, *Adv. Mater.*, 2013, **25**, 4018-4022.
43. M. Dasog, A. I. Carim, S. Yalamanchili, H. A. Atwater and N. S. Lewis, *Nano Lett.*, 2016, **16**, 5015-5021.
44. J. M. Spurgeon, K. E. Plass, B. M. Kayes, B. S. Brunschwig, H. A. Atwater and N. S. Lewis, *Appl. Phys. Lett.*, 2008, **93**, 032112.
45. M. R. Shaner, K. T. Fountaine, S. Ardo, R. H. Coridan, H. A. Atwater and N. S. Lewis, *Energy Environ. Sci.*, 2014, **7**, 779-790.
46. M. R. Shaner, M. T. McDowell, A. Pien, H. A. Atwater and N. S. Lewis, *J. Electrochem. Soc.*, 2016, **163**, H261-H264.
47. O. Khaselev and J. A. Turner, *Science*, 1998, **280**, 425-427.
48. W.-H. Cheng, M. H. Richter, M. M. May, J. Ohlmann, D. Lackner, F. Dimroth, T. Hannappel, H. A. Atwater and H.-J. Lewerenz, *ACS Energy Lett.*, 2018, **3**, 1795-1800.
49. D. Kang, J. L. Young, H. Lim, W. E. Klein, H. Chen, Y. Xi, B. Gai, T. G. Deutsch and J. Yoon, *Nat. Energy*, 2017, **2**, 17043.
50. F. H. Saadi, A. I. Carim, E. Verlage, J. C. Hemminger, N. S. Lewis and M. P. Soriaga, *J. Phys. Chem. C*, 2014, **118**, 29294-29300.

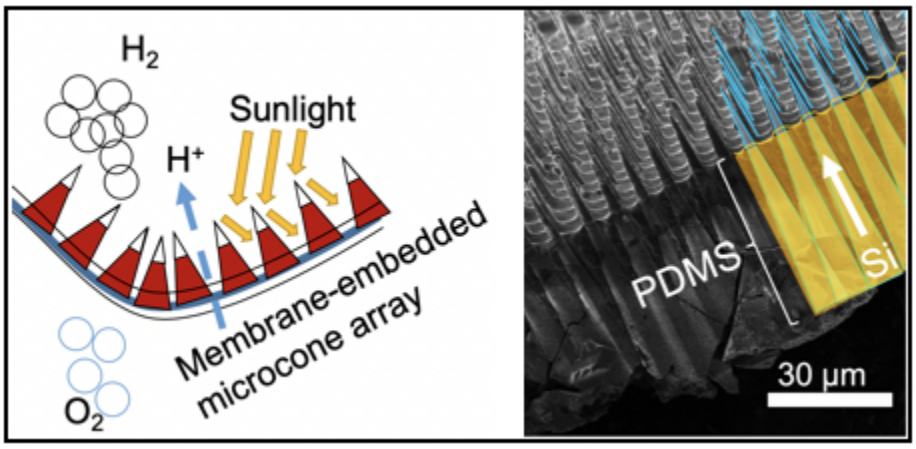
H2
Sunlight
H+
Membrane-embedded
microcone array
O2
PDMS
Si
30 μm